Development and Performance Evaluation of a Cylindrical Cam Shaking Table for Dynamic Centrifuge Modelling

A. Sahare
Advanced Research Laboratories, Tokyo City University, Tokyo, Japan, sahare@tcu.ac.jp

K. Itoh, N. Suemasa, T. Tanaka
Department of Urban and Civil Engineering, Tokyo City University, Tokyo, Japan, itok@tcu.ac.jp, nsuemasa@tcu.ac.jp, ttanaka@tcu.ac.jp

ABSTRACT: This paper presents an operationally simple, cost-effective cylindrical cam shaking table developed for dynamic geotechnical centrifuge modelling and installed on the Mark III beam centrifuge at Tokyo City University. The actuator converts cam rotation into linear table excitation, enabling controlled ramped sinusoidal motions without requiring user-defined input time histories. Building on the underlying mechanical concept, the study emphasises practical characterisation for experimental use, including (i) the cam-follower working mechanism responsible for the ramped sine waveform, (ii) a calibration framework linking applied control voltage to achievable excitation frequency and peak acceleration for different centrifugal accelerations and payload masses, and (iii) frequency-content assessment using first-harmonic representation and time-frequency (Stockwell) analysis to identify the dominant excitation component and secondary higher-frequency content. A capability map is then established in terms of f_{exc}- PGA-payload at 20 g and 50 g, with the stroke limit overlaid, providing users with an experimental operating envelope for designing parametric centrifuge studies that require reliable sinusoidal base shaking.

1 INTRODUCTION AND MOTIVATION

Dynamic geotechnical centrifuge modelling is increasingly used to investigate failure mechanisms, to observe soil-structure interaction at realistic stress levels, and to provide high-quality datasets for validating numerical tools. In these studies, the quality of the imposed base motion is not a secondary detail: repeatable excitation is essential for isolating the effects of model and system parameters (e.g., geometry, stiffness, and boundary conditions) on soil-structure interaction. This requirement is particularly evident in multi-facility benchmarking efforts such as the Liquefaction Experiments and Analysis Projects (LEAP; e.g., Manzari et al., 2018; Zeghal et al., 2018; Sahare et al., 2020; Tobita et al., 2022; Sahare et al., 2024a; Sahare et al., 2024b), where small differences in shaking fidelity and control can influence the achieved input motion and the measured response. Nevertheless, achieving stable, well-controlled shaking in-flight remains a practical limitation for many laboratories, because the actuation and control system must operate reliably under high centrifugal accelerations, variable payload masses, and the geometric constraints of the swinging platform.

Servo-hydraulic shaking systems remain the prevailing solution because they can reproduce arbitrary command histories when the control loop is well tuned (e.g., Madabhushi et al., 2012; Zhou et al., 2020). However, for routine university centrifuge operation, they impose a high barrier in cost, maintenance, and operational complexity, and their performance can be sensitive to test-dependent changes in system dynamics (e.g., payload stiffness, mass distribution, and g-level).

For many centrifuge research questions, a simple sinusoidal input (often applied with a smooth ramp-up and ramp-down) is a purposeful choice: it provides a narrow-band excitation, facilitates frequency and amplitude sweeps, and supports clean attribution of observed geotechnical mechanisms to controlled changes in loading conditions.

The cylindrical cam shaking table developed for the newly installed Mark III geotechnical centrifuge at Tokyo City University (Sahare et al., 2025) was conceived to address this issue. The concept uses a mechanical cam-follower mechanism to transform rotational motion into linear table excitation, producing a ramped sinusoidal waveform without requiring user-defined input time histories. The actuator is driven through the centrifuge's electrical interface, enabling a straightforward experimental workflow in which excitation characteristics are selected via a small set of control parameters.

This paper first summarises the motion-generation principle and the governing cam-follower kinematics that produce the ramped sinusoidal waveform. A calibration and verification procedure is then presented to relate control voltage to achieved excitation frequency and peak acceleration over representative centrifugal accelerations and payload masses. Finally, the achievable operating envelope and motion quality are assessed using repeatability and frequency-content indicators, providing guidance on conditions where secondary spectral components remain small. These results establish a capability description for the cam shaker and support its use in controlled parametric centrifuge studies.

2 SYSTEM DESCRIPTION

Figure 1 shows the Mark III beam-type geotechnical centrifuge facility at Tokyo City University (TCU), which provides the in-flight environment for the present shaking system. The centrifuge has an effective radius of 1.4 m and can achieve a maximum centrifugal acceleration of 100 g, with a maximum payload mass of 500 kg (maximum capacity 10 g-ton). The working platform ("bucket") provides an available plan area of approximately 0.6 m × 0.8 m for mounting model containers and in-flight devices. Power and control signals are transferred between the control room and the rotating arm via slip rings, enabling operation of mounted actuators and acquisition of sensor outputs during flight.

Figure 1. Mark III geotechnical centrifuge facility at TCU.

Figure 2 shows the newly developed cylindrical cam shaking table (500 mm × 270 mm, total mass 71 kg, maximum achievable table displacement = 5 mm) mounted on the arm of the TCU Mark III beam-type centrifuge. The system is designed for operation up to a centrifugal acceleration of 50 g and a maximum mounted sample (payload) mass of 50 kg. The device was conceived as a compact, mechanically driven actuator for one-dimensional horizontal excitation of a model container within the geometric and payload constraints of an in-flight platform, while prioritising repeatability, ease of mounting/unmounting, and a lower construction/maintenance cost burden than more complex servo-hydraulic systems. The excitation principle is based on converting rotational motion into reciprocating linear motion using a cylindrical cam-follower mechanism. The earthquake excitation is generated by the rotation of a cylindrical cam with two waves per rotation. A follower plate is positioned beneath the cam surface (perpendicular to the shaft axis) and is bolt-linked to the main shaking-table platform, so that cam-follower interaction produces a back-and-forth translation of the table along the horizontal axis. The alternating forward-reverse motion of the follower plate and the table platform is generated by the two-wave cam follower geometry, while the observed ramp-up and ramp-down behaviour arises from motor/cam spin-up and spin-down rather than intentionally non-uniform cam-shaft rotation.

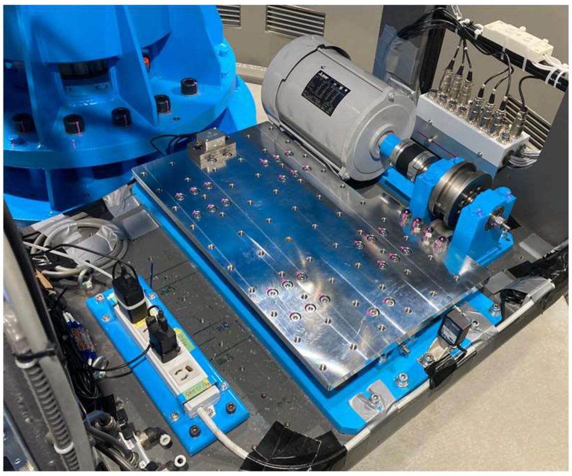

Figure 2. Cylindrical cam shaking table.

A key aspect of the system is its in-flight power and control architecture. The shaking table is operated through the centrifuge's slip-ring interface. Because the centrifuge power-slip-ring terminal block is compatible with AC 100 V, an onboard inverter is mounted on the centrifuge arm to convert the primary supply and deliver 200 V to the motor attached to the shaking table platform. The actuator is driven using the second analogue voltage channel (DC 0-5 V) of the control-slip ring, i.e., a preset voltage is applied as a control input to the inverter/drive (to set motor speed) (rather than commanding an arbitrary displacement history), and the achieved motion is verified by measurement. An automatic switching function is used to coordinate (i) triggering of instrument acquisition (e.g., acceleration, pore pressure, strain) and (ii) initiation of the predetermined sinusoidal excitation; in addition, a separate contact channel can be used to establish a 100 V supply connection for other mounted actuator systems, when required.

In operation, the shaking duration and the pre-/post-trigger delays are specified first, measurement is enabled via the relevant control-slip-ring channel, and the desired excitation level is set by selecting the applied DC voltage (up to 5 V) (together with inverter settings). The cylindrical cam system is then initiated through the automatic switching sequence. Because the actuator is mechanically driven, the excitation is limited to a sinusoidal waveform; moreover, the cam system requires time to spin up and spin down, which naturally produces ascending and descending ramps bracketing the steady sinusoidal cycles.

3 KINEMATIC MODEL

The shaking table generates one-dimensional horizontal excitation by converting the motor-driven cam rotation into reciprocating translation of the table through a cam-follower mechanism. The cylindrical cam used here has two waves per rotation, so one complete cam revolution produces two cycles of table motion. Let the cam angle be $\theta(t)$ and the (instantaneous) angular speed be $\omega(t) = d\theta/dt$. A minimal representation of the cam-imposed table displacement can be expressed as

$$x(t) = Asin(N_w\,\theta(t)), N_w = 2 \quad (1)$$

Where A is the steady displacement amplitude. In practice, A is bounded by the cam stroke (maximum table displacement = 5 mm) but can be smaller depending on the drive level and the shaker-payload interaction. If the cam rotates steadily at $\omega(t) = \omega_0$, the motion reduces to a single-frequency harmonic:

$$x(t) = \mathrm{A}\sin(2\pi f_{exc} t), f_{exc} = \left({N_w}/{2\pi} \right) \omega_o \quad (2)$$

and the corresponding acceleration (during the steady stage) is

$$a(t) = \ddot{x}(t) = -(2\pi f_{exc})^2 A \sin(2\pi f_{exc}\mathrm{t}) \quad (3)$$

In practice, the motor does not instantaneously reach (or stop from) ω_0. Therefore, the waveform can exhibit ramp-up and ramp-down segments, with their prominence depending on the applied voltage (Figure 3), which can be interpreted as periods where $\omega(t)$ (and, effectively, the achieved amplitude) evolves with time. This is the origin of the "ramped sinusoid" observed in the measured acceleration records: a transient stage in which the excitation builds up to an approximately steady sinusoidal motion, followed by a decay stage as the motor spins down.

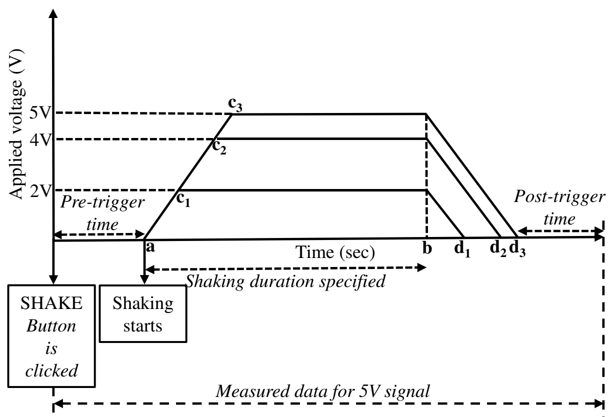

Figure 3. Mechanism of the Cylindrical cam shaking table.

Figure 4 presents the measured horizontal acceleration time histories (model scale) for the 50 kg rigid-box payload at 50 g, obtained at four applied drive voltages (V = 0.88, 1.74, 2.60, 2.80 V). Two consistent features are evident across all voltages:

- Depending on the applied voltage, the measured records show either a weak or negligible ramped envelope (0.88 V) or a clearly defined ramp-up/steady/ramp-down structure (2.60-2.80 V), with the steady segment becoming more distinct as the drive level increases.
- a systematic increase in excitation frequency and the generated acceleration amplitude with increasing applied voltage.

Furthermore, Figure 4 also shows the generated excitation frequency among the different cases. The applied voltage selects the motor/cam speed, which in turn sets the excitation frequency (with the two-wave cam converting cam rotation into two displacement cycles per revolution). For the 50 kg payload at 50 g shown in Figure 4, the steady-stage excitation frequency increases from approximately 4.55 Hz (0.88 V) to 10.80 Hz (1.74 V), 17.07 Hz (2.60 V), and 18.64 Hz (2.80 V), confirming that the applied voltage provides a practical means of selecting the target shaking frequency. The trend also indicates a reduced incremental frequency gain at the highest drive level, which is consistent with the motor-cam system approaching its upper operating range under the present payload and g-level.

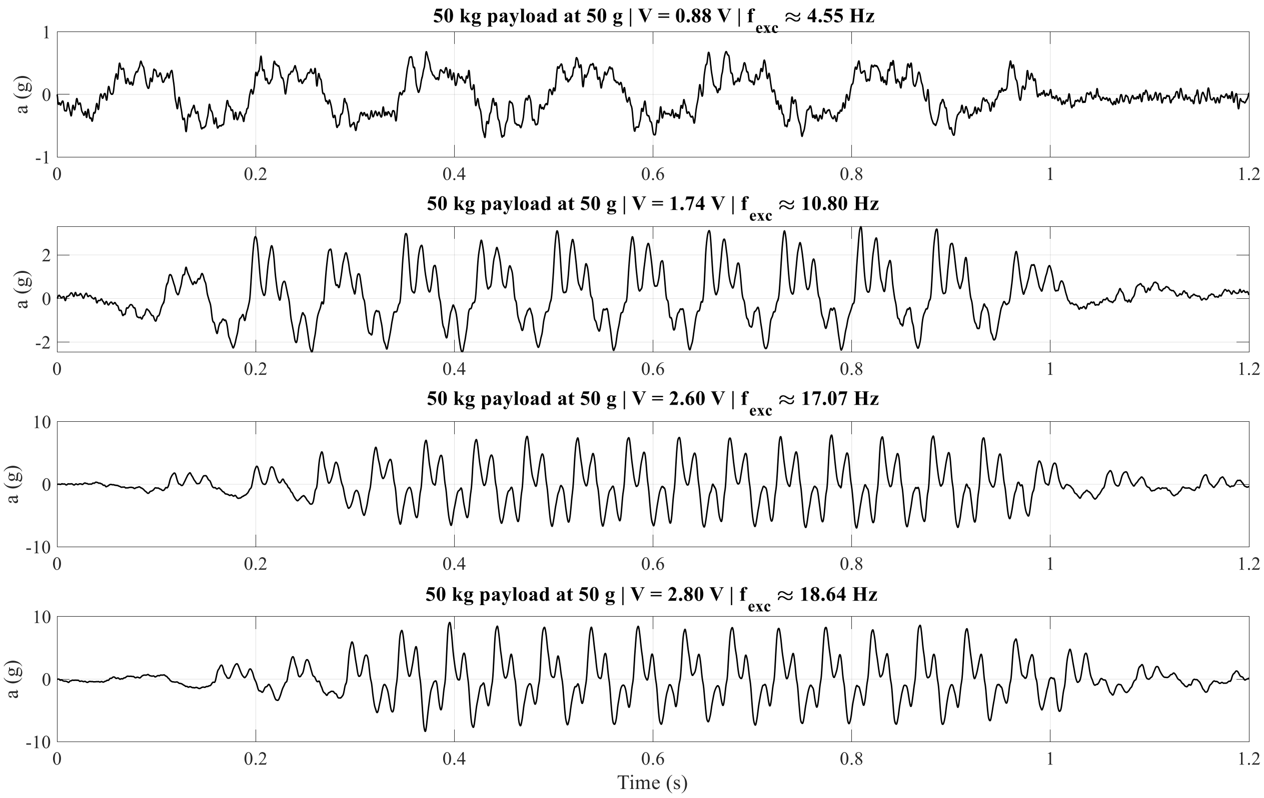

Figure 4. Measured horizontal acceleration time histories (model scale) for a 50 kg rigid-box payload at 50 g centrifugal acceleration, obtained at four applied drive voltages (0.88, 1.74, 2.60, and 2.80 V).

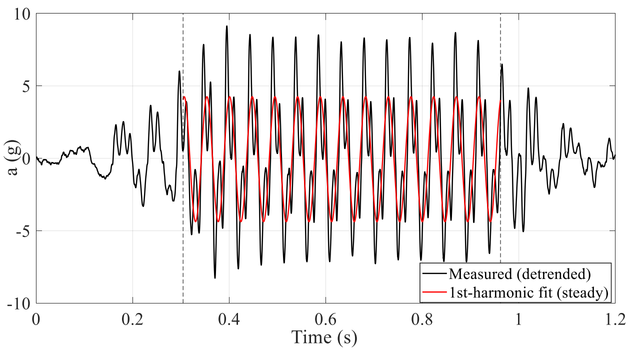

Figure 5. Comparison between the measured acceleration (detrended) and the fitted first-harmonic (fundamental) component during the steady stage for the 2.80 V case (50 kg payload at 50 g; model scale).

While the cam-driven motion is intended to be sinusoidal, the measured acceleration during the steady stage can exhibit non-sinusoidal features (e.g., sharper peaks and slight asymmetry) arising from mechanical aspects such as cam profile details, follower contact conditions, and dynamic interaction between the payload and the shaker assembly. For analytical interpretation and for linking the measured acceleration to an equivalent displacement amplitude, it is useful to isolate the fundamental (first-harmonic) component over the steady window. Figure 5 compares the detrended measured acceleration for the V = 2.80 V case with a first-harmonic fit of the form.

$$a(t) = \hat{a}\sin(2\pi f_{exc} + \phi) \tag{4}$$

Where f_{exc} = 18.64 Hz is fixed from the steady-stage frequency estimate, and $\hat{a}$ and ϕ are obtained by least-squares fitting over the steady interval. The comparison shows that the fitted harmonic reproduces the dominant oscillatory trend and phase of the measured signal during the steady stage. The remaining mismatch, most visibly at the sharp peaks, is consistent with higher-harmonic content and does not contradict the use of the first harmonic as an equivalent sinusoidal representation of the imposed motion. The first-harmonic representation is particularly useful because it provides a direct mapping between the measured acceleration amplitude and the implied displacement amplitude:

$$A = {\hat{a}}\Big/{(2\pi f_{exc})^2} \tag{5}$$

This enables a simple check against the mechanical displacement limit (maximum table displacement) and provides a compact descriptor of input motion for controlled parametric centrifuge studies.

4 SHAKING CONTROL PERFORMANCE: TIME-FREQUENCY BEHAVIOUR AND OPERATING ENVELOPE

Figure 6 presents Stockwell (S-transform) time-frequency magnitude maps for the four operating conditions at V = 2.8 V, covering two payload masses (36 and 50 kg) and two centrifugal acceleration levels (20g and 50g). Across all cases, the response is characterised by a clear ramp-up followed by steady and ramp-down structure: a dominant narrow-band component emerges during the ramp-up, stabilises during the steady stage, and then decays during spin-down. The overlaid ridge indicates the extracted dominant-frequency trajectory, highlighting that the excitation frequency becomes nearly constant once the system reaches the steady regime. Minor differences between the dominant frequency identified from the Stockwell ridge and the frequency inferred from response spectra (or Fourier-based estimates) are expected because the Stockwell transform provides a time-localised dominant-frequency trace that is sensitive to windowing and ramp transients, whereas response spectra/Fourier analyses reflect frequency content integrated over a selected time window and processing choices (e.g., detrending, filtering, and window length).

In addition to the dominant band at f_{exc}, Figure 6 shows secondary higher-frequency content that becomes more evident once the steady stage is established. A characteristic feature is energy concentrated at approximately three times the excitation frequency ($3f_{exc}$) which is consistent with observations reported for servo-hydraulic shaker systems in centrifuge facilities, where higher-harmonic components can arise from actuator/structure compliance and non-ideal force transmission (Kutter et al., 2018; Zhou et al., 2020). For the cam-driven system, these components are plausibly associated with cam-follower contact dynamics, mechanical compliance, and slight non-sinusoidal waveform distortion during the steady stage, consistent with the comparative observations of higher-frequency components reported for centrifuge shaker inputs across facilities (Sahare et al., 2022; Barrios et al., 2021; Ibuki et al., 2022). Importantly, the time–frequency view allows this behaviour to be linked to when it activates (primarily during steady excitation), rather than simply noting its presence in a global spectrum.

Figure 7 summarises the achievable operating space of the cam shaker using a capability map expressed in terms of excitation frequency f_{exc}, peak ground acceleration (PGA), and payload (36 and 50 kg), shown for a centrifugal acceleration of (a) 20 g and (b) 50 g. Each marker corresponds to an operating point obtained at a given applied control voltage, and the labels indicate the voltage level. The map highlights the fundamental control trend: increasing applied voltage increases both f_{exc} and PGA, reflecting the voltage-controlled motor speed and the resulting increase in excitation intensity.

The capability map also shows the expected payload effect: for a given voltage level, larger payload tends to reduce achievable PGA, while the excitation frequency remains comparatively less sensitive because it is primarily governed by the commanded motor/cam speed. The translucent stroke-limit surface indicates the kinematic constraint imposed by the maximum table displacement (5 mm), providing a practical boundary for selecting test conditions. Together, Figure 7 provides a compact “use chart” for experiment planning: it links the selectable control voltage to the resulting f_{exc} -PGA-payload combination at the target g-level, and clarifies how operating points shift with payload and centrifugal acceleration.

5 CONCLUSIONS

This study presented a simplistic compact cylindrical cam shaking table developed for the Mark III beam centrifuge at Tokyo City University. The cam-follower mechanism generates a ramped sinusoidal waveform in which the applied control voltage governs the motor/cam speed and therefore the achieved excitation frequency and peak acceleration. Measured acceleration records confirmed a systematic increase in both f_{exc} and PGA with increasing voltage and showed that a first-harmonic representation captures the dominant steady-stage motion for practical conversion between acceleration and equivalent displacement amplitude. Stockwell time-frequency analysis demonstrated consistent ramp-up/steady/ramp-down behaviour and identified secondary higher-frequency content that becomes more evident during steady excitation. Finally, a capability map was established in terms of f_{exc}-PGA-payload at 20 g and 50 g, providing a practical operating envelope for selecting input motions for parametric centrifuge studies where stable, repeatable sinusoidal shaking is required.

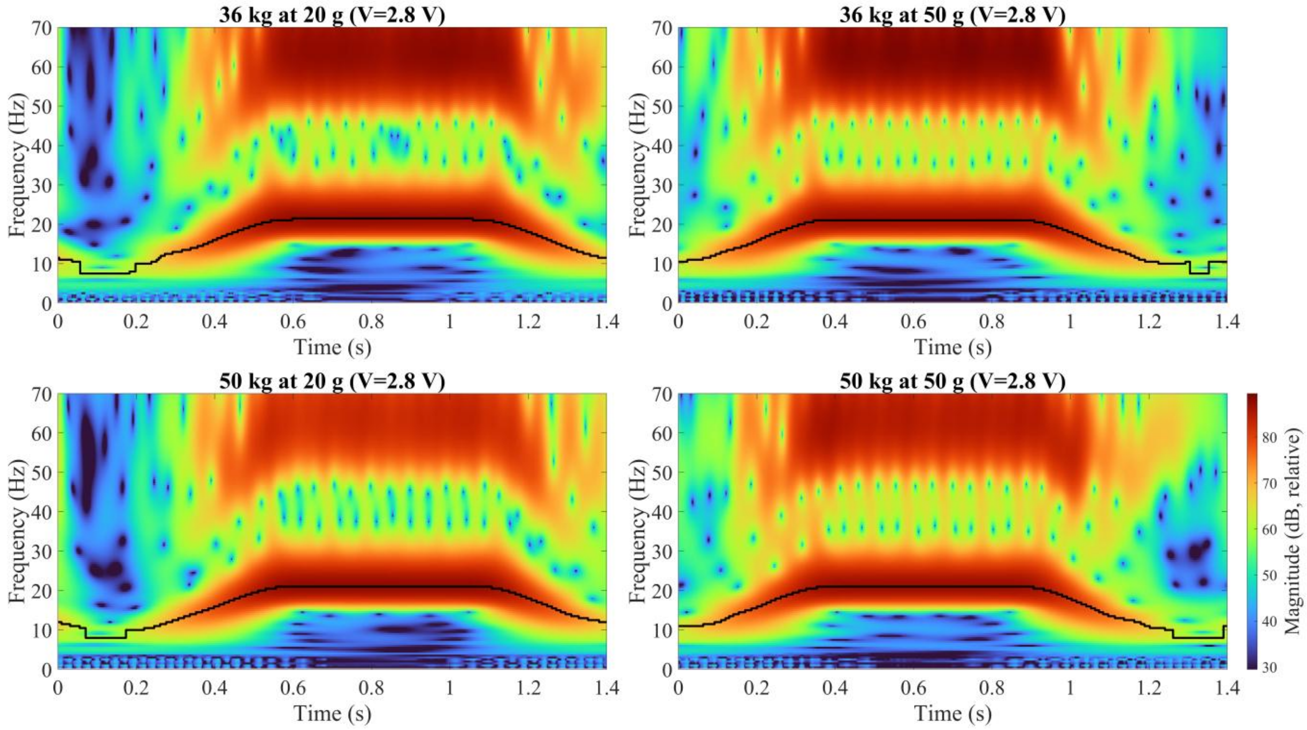

Figure 6. Stockwell (S-transform) time-frequency magnitude maps (V = 2.8 V) for four centrifuge operating conditions: payload mass = 36 and 50 kg at centrifugal acceleration levels of 20g and 50g. Colour contours indicate relative magnitude (dB), and the overlaid curve shows the extracted dominant-frequency ridge.

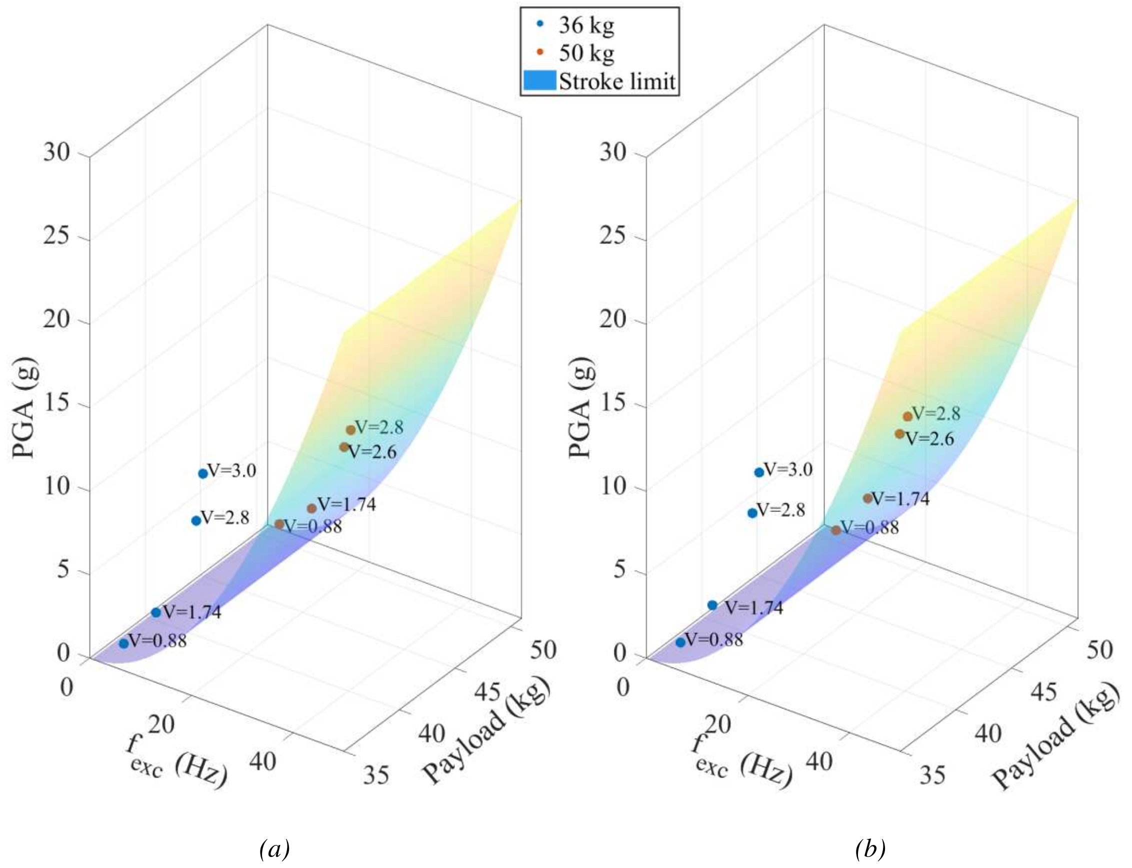

Figure 7. Capability map of the cam shaker showing the achievable operating space in terms of excitation frequency f_{exc}, peak ground acceleration (PGA), and payload (36 and 50 kg) at a centrifugal acceleration of (a) 20 g and (b) 50 g, with the 5-mm stroke limit surface overlaid; labels indicate the applied voltage.

ACKNOWLEDGEMENTS

The TCU Mark III geotechnical centrifuge facility and the cylindrical cam mechanical shaking table actuator were developed with the support of Tokyo City University under the introduction of 'Large Research Equipment and Facilities' for the development of research infrastructure. The authors are thankful to Mr. Mitsuyoshi Torita and Mr. Ryoma Takeoka for their assistance in the development of the centrifuge equipment and the mechanical shaker. The authors are also thankful to Mr. Kazuya Sano for his assistance during the centrifuge experiments reported in this paper.

REFERENCES

Barrios, G., Uemura, K., Kikkawa, N., et al. (2021). Dynamic response of standalone and adjacent footing on saturated sand. *Soil Dynamics and Earthquake Engineering*, 143: 106584. http://doi.org/10.1016/j.soildyn.2021.106584.

Ibuki, R., Doi, T., Izawa, J., Uemura, K., and Sreng, S. (2022). High speed observation on damage process of embankments during earthquakes in a centrifugal acceleration field. In *Proceedings of the 10th International Conference on Physical Modelling in Geotechnics (ICPMG 2022)*, Korea, pp. 912–915.

Kutter, B.L., Carey, T.J., Hashimoto, T., et al. (2018). LEAP-GWU-2015 experiment specifications, results, and comparisons. *Soil Dynamics and Earthquake Engineering*, 113: 616–628. http://doi.org/10.1016/j.soildyn.2017.05.018.

Madabhushi GSP, Haigh SK, Houghton NE and Gould E (2012) Development of a servo-hydraulic earthquake actuator for the Cambridge turner beam centrifuge. *International Journal of Physical Modelling in Geotechnics*, 12(2): 77–88. https://doi.org/10.1680/ijpmg.11.00013.

Manzari, M.T., El Ghoraiby, M., Kutter, B.L., et al. (2018). Liquefaction experiment and analysis projects (LEAP): summary of observations from the planning phase. *Soil Dynamics and Earthquake Engineering*, 113: 714–743. http://doi.org/10.1016/j.soildyn.2017.05.015.

Sahare, A., Tanaka, Y., and Ueda, K. (2020). Numerical study on the effect of rotation radius of geotechnical centrifuge on the dynamic behavior of liquefiable sloping ground. *Soil Dynamics and Earthquake Engineering*, 138: 106339. http://doi.org/10.1016/j.soildyn.2020.106339.

Sahare, A., Ueda, K., and Uzuoka, R. (2022). Influence of the sloping ground conditions and the subsequent shaking events on the pile group response subjected to kinematic interactions for a liquefiable sloping ground. *Soil Dynamics and Earthquake Engineering*, 152: 107036. https://doi.org/10.1016/j.soildyn.2021.107036.

Sahare, A., Choi, G.C., and Ueda, K. (2024a). Role of initial static shear on the cyclic response of saturated backfill retained by a sheet-pile wall: Insights from the strain space multiple mechanism model. *Soil Dynamics and Earthquake Engineering*, 179: 108542. http://doi.org/10.1016/j.soildyn.2024.108542.

Sahare, A., and Ueda, K. (2024b). Dynamic centrifuge modeling to investigate the deformation mechanism of an embedded cantilever retaining wall with submerged backfill conditions. *Soil Dynamics and Earthquake Engineering*, 179: 108510, https://doi.org/10.1016/j.soildyn.2024.108510.

Sahare, A., Sano, K., Itoh, K., Suemasa, N., Tanaka, T., Torita, M., and Takeoka, R. (2025). Development of a novel cylindrical cam shaking table for geotechnical centrifuge modelling. *International Journal of Physical Modelling in Geotechnics*, 25(2): 66–85. http://doi.org/10.1680/jphmg.24.00032.

Tobita, T., Ueda, K., Vargas, R.R., et al. (2022). LEAP-ASIA-2019: validation of centrifuge experiments and the generalized scaling law on liquefaction-induced lateral spreading. *Soil Dynamics and Earthquake Engineering*, 157: 107237. http://doi.org/10.1016/j.soildyn.2022.107237.

Zeghal, M., Goswami, N., Kutter, B.L., et al. (2018). Stress-strain response of the LEAP-2015 centrifuge tests and numerical predictions. *Soil Dynamics and Earthquake Engineering*, 113: 804–818. http://doi.org/10.1016/j.soildyn.2017.10.014.

Zhou, Y.-G., Meng, D., Ma, Q., et al. (2020). Frequency response function and shaking control of the ZJU-400 geotechnical centrifuge shaker. *International Journal of Physical Modelling in Geotechnics*, 20(2): 97–117. http://doi.org/10.1680/jphmg.19.00029.